Beam Spoiling Correction for Spaceborne Microwave Radiometers Using the Two-Point Vicarious Calibration Method

Darren S. McKague, *Member, IEEE*, Christopher S. Ruf, *Fellow, IEEE*, and John J. Puckett, *Student Member, IEEE*

***Abstract*—The vicarious warm and cold calibration techniques are combined to provide an end-to-end two point calibration method for spaceborne microwave radiometers. The method uses stable external calibration sources to permit an end-to-end calibration of the complete radiometer, including its primary antenna. Both gain and offset corrections to the radiometer calibration can be computed since vicarious reference points at both the cold and warm ends of the measurement range are available. The method is demonstrated using the WindSat radiometer. Calibration errors are found which vary with azimuthal scan position in a manner that suggests that the cause is beam spoiling from on-board spacecraft obstructions. The impact on gain and offset calibration errors of the on-board obstructions can be determined from the vicarious calibration. This information is used to characterize the beam spoiling–specifically to determine the decrease in the antenna's beam efficiency and the mean brightness temperature entering the far sidelobes of the antenna, both as functions of azimuthal scan position. With this characterization available, a calibration correction algorithm can be constructed that is based on the root cause of the problem.**

***Index Terms*—Calibration, microwave radiometry.**

I. Introduction

IF PASSIVE microwave data from multiple instruments are to be combined for use in, for example, the Global Precipitation Measurement (GPM) mission, the data must be well calibrated in both an absolute and a relative sense. That is the goal of the GPM Inter-satellite Calibration Working Group (ICWG) [1]. The work presented here is part of the ICWG effort. Both the absolute radiometric calibration of individual instruments and the relative calibration between instruments are significantly improved if the nuances and imperfections of each instrument are well understood.

The first step in the process is to understand the calibration of each individual radiometer within the ICWG constellation of radiometers. Calibration errors for each radiometer must be determined and when possible, corrections must be developed. These errors are often linearly dependent on brightness temperature, in which case they can be characterized by a gain and an offset term. These two terms can be determined by the measurement of two known brightness temperature values, preferably at the cold and the warm ends of the measurement dynamic range. This paper develops such a method, combining the vicarious cold method of Ruf [2], [3] with the vicarious warm method of Brown and Ruf [4] to provide an end-to-end (through the main reflector) two-point calibration using stable and external on-Earth targets. The method is demonstrated using WindSat data for which beam-spoiling due to on-board obstructions in the feedhorn sidelobes is corrected. The method is also used to correct for differences from nominal instrument Earth incidence angles (EIA) due to roll and pitch offsets of the instrument platform.

Manuscript received November 1, 2009; revised March 9, 2010 and July 3, 2010; accepted July 20, 2010. Date of publication October 21, 2010; date of current version December 27, 2010. This work was supported in part by the NASA Grant NNX07AD69G.

D. S. McKague and J. J. Puckett are with the Department of Atmospheric, Oceanic and Space Sciences, University of Michigan, Ann Arbor, MI 48109 USA (e-mail: dmckague@umich.edu; puckjohn@umich.edu).

C. S. Ruf is with the Space Physics Research Laboratory, Department of Atmospheric, Oceanic, and Space Sciences, University of Michigan, Ann Arbor, MI 48109 USA (e-mail: cruf@umich.edu).

Color versions of one or more of the figures in this paper are available online at http://ieeexplore.ieee.org.

Digital Object Identifier 10.1109/TGRS.2010.2068052

II. Two-Point Vicarious Calibration

A. WindSat Data Characteristics

Data from the WindSat instrument are used to demonstrate the method. Characteristics of the WindSat platform are shown in Table I. WindSat is in a sun-synchronous orbit, with local times at the antenna footprint near 6 A.M. and 6 P.M. [5]. Data from July 2005 to June 2006, provided as part of the GPM ICWG effort, were analyzed. Only vertical (V) and horizontal (H) polarization channels were used. Although WindSat makes observations in both the forward and backward scanning directions with respect to the orbital velocity, only forward scanning data were used and were limited to the scan positions over which all channels observe. Data were remapped to the resolution of the 18.7 GHz channel with along-scan spacing of every fourth 37.0 GHz V, H-pol observation. The data were limited in polarization and scan position, and remapped to a common spatial grid for simplicity of processing within the ICWG. The intention was to provide an initial data set for developing the intercalibration process. Limiting and remapping the dataset do not affect the validity of the processes described in this paper. The data were corrected for polarization rotation due to attitude offsets, spillover, and antenna pattern corrections, although neither scan position dependent bias correction nor EIA correction for attitude offsets were applied prior to ICWG processing. These corrections are included in the standard WindSat data but were left out so that the ICWG could develop independent corrections.

TABLE I
WINDSAT CHARACTERISTICS. POLARIZATIONS ARE VERTICAL (V), HORIZONTAL (H), PLUS AND MINUS 45 DEGREE LINEAR (±45), LEFT HAND CIRCULAR (LC) AND RIGHT HAND CIRCULAR (RC). ONLY V AND H POLARIZATION CHANNELS WERE USED IN THIS PAPER, WITH ALL CHANNELS RE-GRIDDED TO THE RESOLUTION OF THE 18.7 GHz CHANNEL

Frequency (GHz)	Polarization	Instantaneous Field of View (km)	Nominal Earth Incidence Angle (deg)	Incidence Angle Range Including Attitude Effects (deg)	Channel NEDT (Kelvins)
6.8	V, H	40x60	53.53	53.23-53.83	0.63
10.7	V, H, ±45, lc, rc	25x38	49.91	49.61-50.21	0.44
18.7	V, H, ±45, lc, rc	16x27	55.35	55.05-55.65	0.44
23.8	V, H	12x20	53.0	52.7-53.3	0.60
37.0	V, H, ±45, lc, rc	8x13	53.0	52.7-53.3	0.42

TABLE II
MEAN AND STANDARD DEVIATION OF RETRIEVED VICARIOUS COLD AND WARM CALIBRATION T_b's COMPUTED OVER ALL MONTHS AND ALL SCAN POSITIONS

Frequency (GHz)	Mean Vicarious Cold Cal. T_b, V-Pol/H-pol (K)	Standard Deviation of Cold Cal. T_b, V-Pol/H-pol (K)	Mean Vicarious Warm Cal. T_b, V-Pol/H-pol (K)	Standard Deviation of Warm Cal. T_b, V-Pol/H-pol (K)
6.8	151.4/75.0	1.2/0.3	279.7/278.1	1.4/1.1
10.7	152.1/83.9	0.3/0.2	282.6/281.1	0.8/0.8
18.7	181.7/94.2	1.1/1.2	281.1/285.6	1.0/1.0
23.8	187.4/109.6	2.8/3.8	287.5/286.9	0.7/0.7
37.0	204.3/128.0	0.9/0.6	284.4/283.5	0.8/0.8

B. Vicarious Cold Calibration

The vicarious cold calibration technique of Ruf [2] is used to provide the cold point in the two-point vicarious calibration. Data were analyzed to compute vicarious calibration brightness temperatures (T_b's) as a function of WindSat scan position for each month. These monthly results were then averaged to compute yearly mean vicarious cold calibration T_b's as a function of scan position. The means and standard deviations of the retrieved vicarious cold and warm calibration T_b's for each channel are shown in Table II. The difference between the yearly mean vicarious cold calibration T_b at each scan position and the mean of the 10 scan positions around the center of scan (scan position 35) was computed to determine scan position dependent biases in the data. Results are shown in Fig. 1.

Two significant features are evident in Fig. 1: large edge-of-scan biases in the 6.8 GHz and 23.8 GHz data, and a polarization dependent slope in the cross scan bias. The edge-of-scan biases are likely due to on-board obstructions from nearby hardware such as the external warm and cold loads, which enter the respective feed-horn field of view at either end of the Earth viewing portion of the WindSat scan [6]. Section II-D examines this calibration error in greater detail.

For the scan position dependent bias slope, the magnitude is larger and opposite in sign for vertical polarization (V-pol) than for horizontal (H-pol). Over ocean brightness temperatures, and hence the vicarious cold calibration T_b's, are sensitive to small changes in EIA [2], [3]. This sensitivity is higher and opposite in sign for V-pol than for H-pol. This is demonstrated in Fig. 2, which shows the theoretical vicarious cold calibration T_b as a function of EIA for the WindSat V and H-pol channels using the ocean emissivity model of [7].

EIA will vary from its nominal value in a systematic and predictable manner as a function of scan position for any roll or pitch attitude offsets in the instrument [8]. Combining this relationship with the model of ocean brightness temperatures

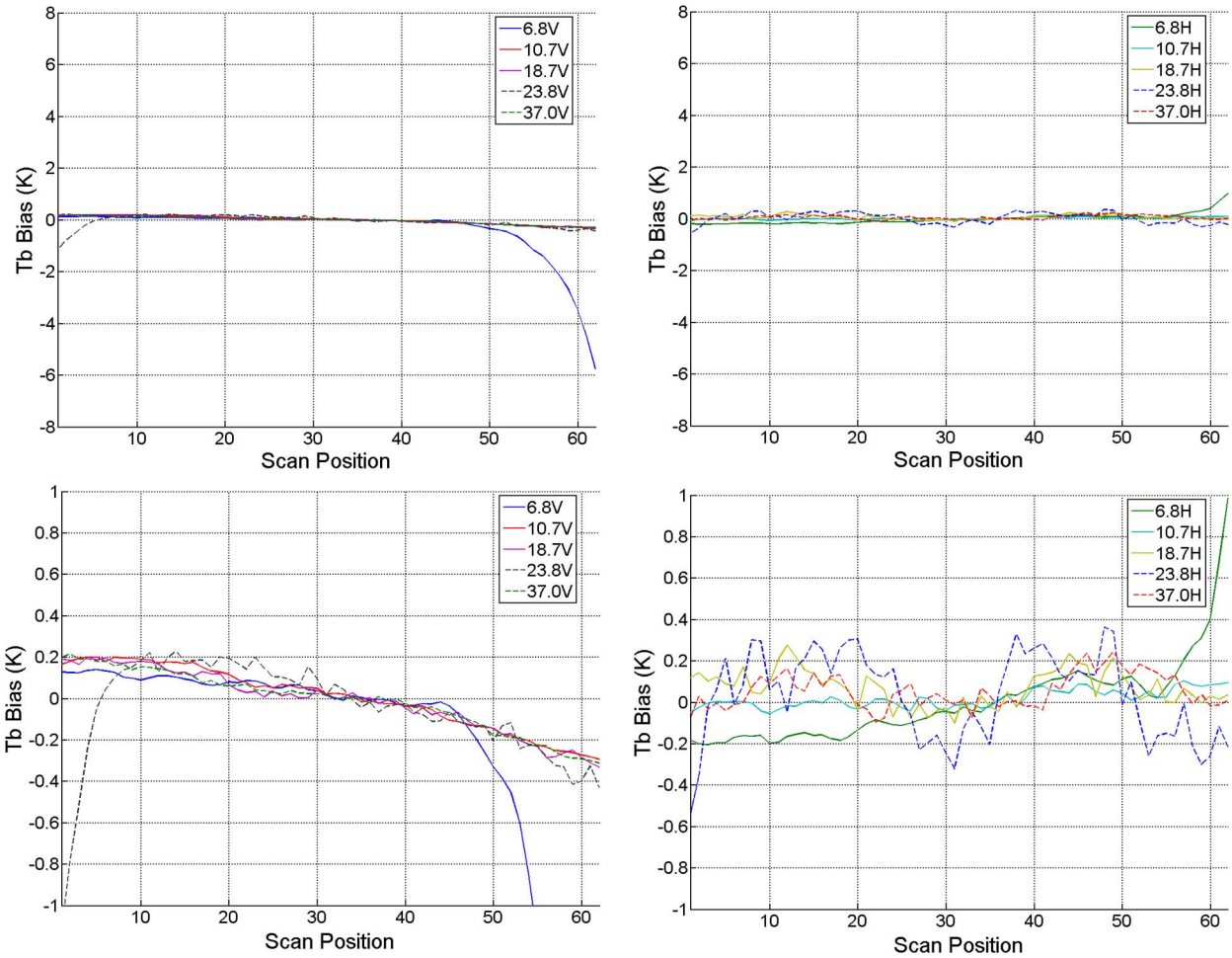

Fig. 1. Biases of WindSat vicarious cold brightness temperatures relative to center of scan for vertical polarization channels (left) and horizontal polarization channels (right). The top plots are scaled to show edge-of-scan biases at 6.8 and 23.8 GHz, while bottom plots are scaled to show smaller scale variability. Biases are from vicarious cold calibration T_b's retrieved from fits to cumulative distribution functions created from histograms containing approximately 10 000 observations per histogram bin. See [2] for vicarious cold calibration T_b retrieval details.

as a function of EIA from [7], the scan position dependent biases in Fig. 1 have been used to determine roll and pitch offsets that are consistent with the data. This was accomplished by finding the roll and pitch offsets that minimize the rms difference between measured and modeled T_b's across the scan (excluding the problematic edge-of-scan regions). Fig. 3 shows the resulting rms difference as a function of roll and pitch offset; the difference is minimized at a roll offset of -0.16° and a pitch offset of 0.2°. This agrees well with the results of [9] and [10], which use similar analysis of over ocean T_b's and geolocation errors to derive WindSat roll, pitch offsets of -0.15°, 0.18° and -0.16°, 0.18°, respectively. Figs. 4 and 5 show the V-pol and H-pol cross scan biases with this attitude/EIA offset. The effect is much clearer for V-pol than for H-pol due to the increased sensitivity to EIA changes and the decreased residual atmospheric "noise" at V-pol relative to H-pol. H-pol T_b's shows larger residual atmospheric variability due to the higher reflectivity at H-pol over ocean which leads to larger atmospheric contributions to observed T_b's from reflected downwelling atmospheric radiation. The resulting scan position dependent T_b biases with corrected EIAs are less than 0.4 K, except for the scan edges at 6.8 and 23.8 GHz.

C. Vicarious Warm Calibration

As with the vicarious cold calibration, the data have been analyzed using the vicarious warm calibration method of Brown and Ruf [4] using Global Data Assimilation System (GDAS) data [11] to model the atmospheric contribution to the measured brightness temperatures. The albedo of the rainforest in [4] was modeled as a linear function of frequency from 18.7 GHz to 37.0 GHz; the albedo of vegetation in this frequency range is expected to increase approximately linearly with frequency. WindSat adds channels at 6.8 and 10.7 GHz; over this range, the albedo is approximated more accurately with a quadratic function of frequency (see, e.g., Fig. 3 in [12]). For the results shown here, the albedo (a) is modeled as

$$a = a_0 + a_1 f + a_2 f^2 \tag{1}$$

where f is the frequency in GHz. The albedo minimum is fixed at 10.7 GHz, so the quadratic term a_2 can be solved for, reducing the dimensionality of the retrieval space

$$a_2 = -a_1/(2 * 10.7). \tag{2}$$

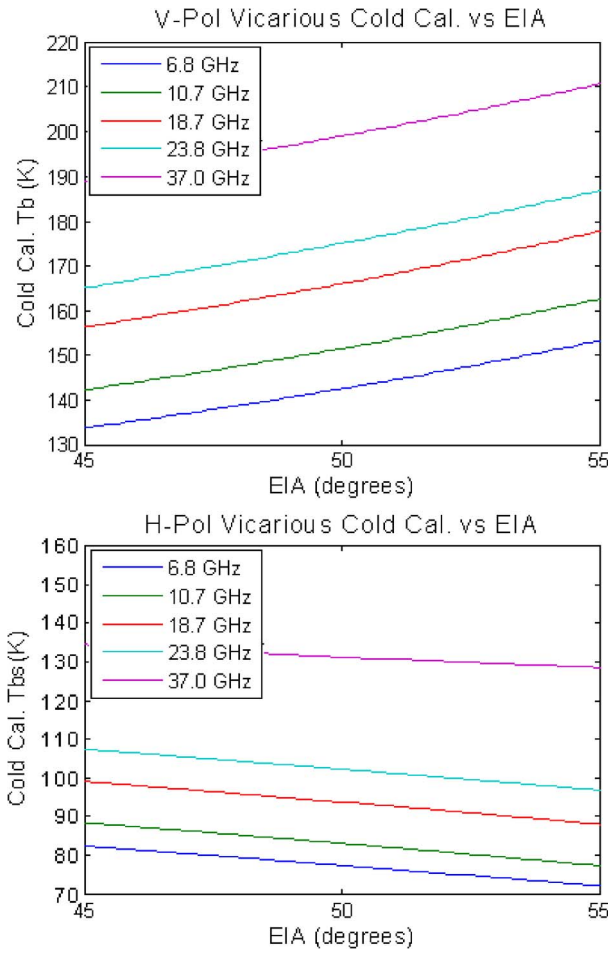

Fig. 2. Dependence of the vicarious cold calibration brightness temperatures for the WindSat channels on EIA. The vertical polarization channels are shown on top and the horizontal polarization channels are shown on bottom.

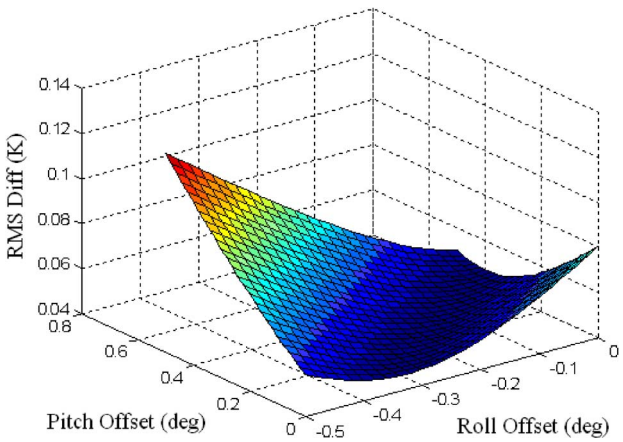

Fig. 3. Rms difference between the observed and modeled vicarious cold T_b's as a function of spacecraft roll and pitch offsets. The minimum is at a roll offset of $-0.16°$ and a pitch offset of $0.2°$.

The vicarious warm biases for WindSat as a function of scan position relative to the center of scan are shown in Fig. 6. As with the cold data, the mean of the center 10 positions was used as the reference. Since the vicarious warm observations are made over land, the sensitivity to EIA and hence to attitude offsets are significantly reduced. However, the magnitudes of the edge-of-scan biases at the 6.8 GHz and 23.8 GHz channels

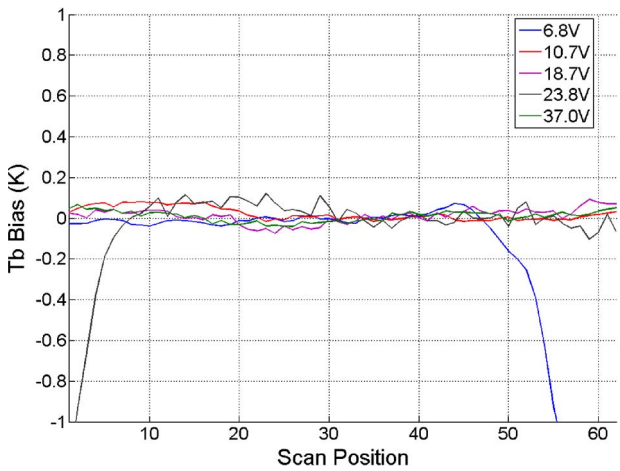

Fig. 4. Vicarious cold calibration vertical polarization biases with correction for instrument roll and pitch offsets.

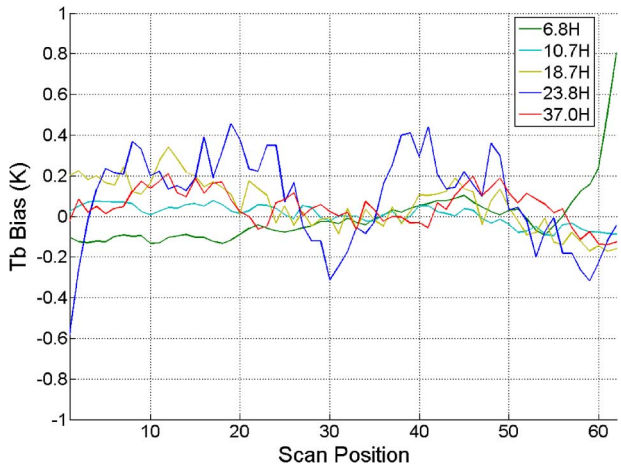

Fig. 5. Vicarious cold calibration horizontal polarization biases with correction for instrument roll and pitch offsets.

are larger than the corresponding over ocean bias. As is shown in the next section, the effective radiating temperatures of the edge-of-scan obstructions are relatively low ($<$ 95 K). The contrast between main beam T_b and obstruction T_b is higher for the vicarious warm T_b (around 280 K—see Table II) than for the vicarious cold T_b's (between 75 and 205 K depending upon channel—see Table II), resulting in a higher bias for the vicarious warm calibration T_b's.

D. Beam Spoiling Correction

The antenna temperature T_A measured by a radiometer can be written in general as

$$T_A = \int_{4\pi} T_b(\Omega')G(\Omega', \Omega)d\Omega' \tag{3}$$

where $T_b(\Omega')$ is the brightness temperature in the direction of the element of solid angle Ω' and $G(\Omega, \Omega')$ is the gain of the antenna in the direction Ω' for an antenna pointing in the direction Ω [13]. The antenna gain is normalized to unity

$$\int_{4\pi} G(\Omega', \Omega)d\Omega' = 1. \tag{4}$$

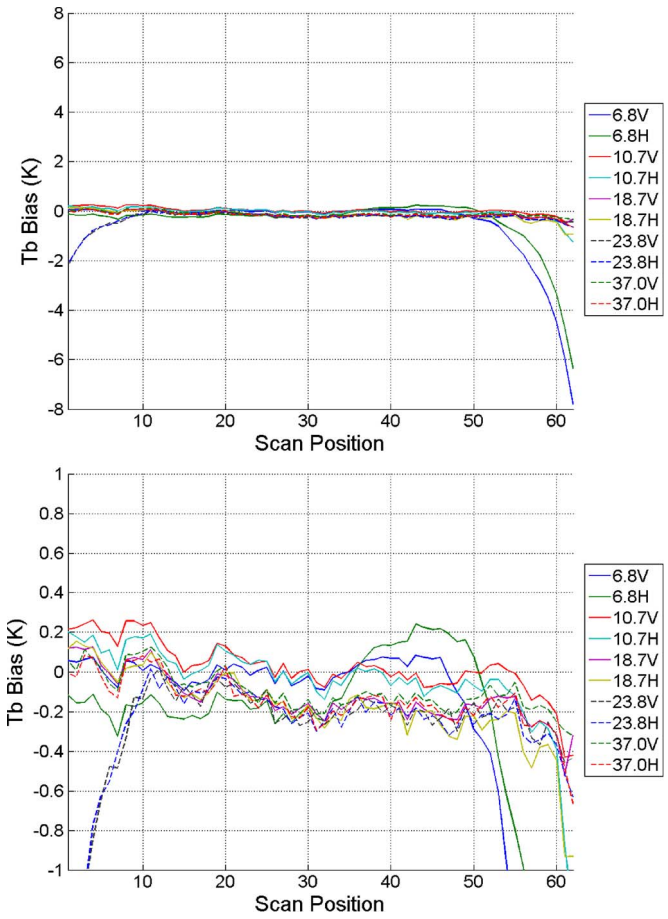

Fig. 6. Biases of WindSat vicarious warm calibration brightness temperatures relative to center of scan. Top and bottom plots are the same data shown with two different T_b scales to show the edge-of-scan biases, and the relative scale and variability of biases for all channels, respectively. Biases are from vicarious warm calibration T_b's retrieved from approximately 27 000 observations per channel. See [4] for vicarious warm calibration T_b retrieval details.

The goal of antenna pattern correction is to estimate the brightness temperature within the main beam of the antenna, $T_{b,mb}$, given measurements of T_A, measurements of G (e.g., preflight characterization of the antenna), and estimates of the brightness temperature of sources outside the main beam (i.e., in the side-lobes). The integral in (4) can be broken into ranges of solid angle for the main beam and each of the side-lobe sources $(1, 2, \ldots)$

$$T_A = \int_{mb} T_{b,mb} G(\Omega', \Omega) d\Omega' + \int_{1} T_1 G(\Omega', \Omega) d\Omega' + \int_{2} T_2 G(\Omega', \Omega) d\Omega' + \ldots \quad (5)$$

If the brightness of the sources in each range of solid angle is relatively uniform, (5) can be approximated with a sum of the form

$$T_A = T_{b,mb} * f_{mb} + T_1 * f_1 + T_2 * f_2 + \ldots \quad (6)$$

where the beam fractions $f_{mb,1,2,\ldots}$ are integrals of the antenna gain G over the corresponding range of solid angle. The sum of all beam fractions is one since G is normalized given (4).

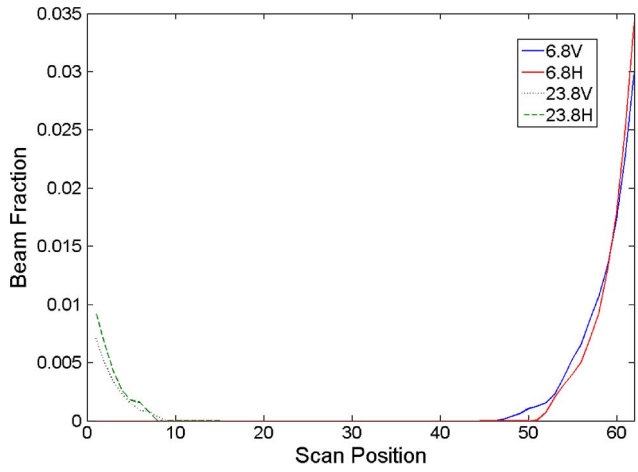

Fig. 7. Beam fractions of the edge-of-scan interferers [f_{obst} in (3)] as a function of scan position for 6.8 and 23.8 GHz.

TABLE III
EFFECTIVE RADIATING TEMPERATURES OF THE EDGE-OF-SCAN INTERFERERS [$T_{b,obst}$ IN (3)] SEEN IN FIG. 1, FIGS. 4–6

Channel	$T_{b,obst}$ (K)
6.8V	2.7
6.8H	94.4
23.8V	2.7
23.8H	78.2

The edge-of-scan biases seen on WindSat are likely caused by obstructions emitting and scattering radiation into the feed horns' fields of view. While a general side-lobe correction has been performed, the brightness temperatures used in this study have not been corrected for these obstructions. To perform this final correction, we break down the antenna temperature as an obstruction free and obstructed component in the same way we formulated the side-lobe contributions in (6)

$$T_A = T_{b,mb} * (1 - f_{obst}) + T_{b,obst} * f_{obst} \quad (7)$$

where f_{obst} is the beam fraction of the obstructions and $T_{b,obst}$ is the effective brightness temperature of the obstructions. Estimating $T_{b,obst}$ and f_{obst} requires observations of T_A with known $T_{b,mb}$; these are taken from the vicarious cold and warm calibration data. From the vicarious calibration observations, $T_{b,mb}$ is estimated at the edge of scan from the center of scan vicarious brightness temperatures with corrections for instrument attitude offsets as described above. Since the beam patterns vary from channel to channel, separate estimates of $T_{b,obst}$ and f_{obst} are made for each channel. It is assumed that $T_{b,obst}$ is the same for all edge-of-scan positions for a given channel and that only f_{obst} varies with scan position. Results are shown in Fig. 7 and Table III. With these and (7), estimates of the obstruction-free main beam T_b's can be made. This beam-spoiling correction is estimated from observations at either end of the dynamic range of observed T_b's, i.e. from T_b's ranging

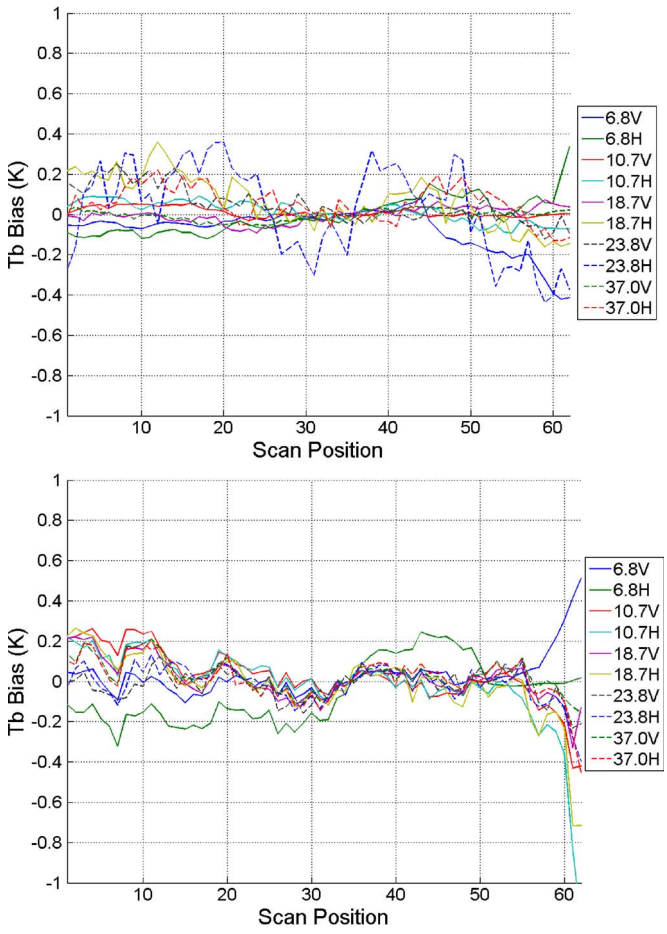

Fig. 8. WindSat scan position dependent biases for the vicarious cold (top) and vicarious warm (bottom) calibration T_b's with corrections for attitude offsets and edge-of-scan interference at 6.8 and 23.8 GHz.

from the coldest observed to close to the warmest observed. The estimated corrections should, therefore, be accurate over a wide range of T_b's between these two extremes.

Edge-of-scan biases have been noted on a number of conically scanning radiometers, including WindSat, and are believed to be due to scattering and/or emission from on-board sources such as the on-board hot load and cold sky reflector into the radiometer sidelobes [6], [14]. The 6.8 GHz and 23.8 GHz feedhorns on WindSat are the farthest from the center of the feedhorn bench, making them the most likely to show edge-of-scan interference from the on-board calibration loads (see Figs. 2 and 3 of [5]). They are also at opposite ends of the feedhorn bench which explains why the edge-of-scan interference for each is seen at opposite ends of the scan. The beam fractions of the interferers increase as the feedhorns draw nearer to the edge of scan as expected for an interferer at the edge of the scan. Since the V and H-pol beam patterns for a given feedhorn differ, the effective beam fraction and radiating temperature of the interferers for V and H-pol differ.

Biases as a function of scan position for corrected data, with both attitude offset and 6.8 and 23.8 GHz edge-of-scan interference corrections, are shown in Fig. 8 for both the vicarious cold (top) the vicarious warm (bottom) calibration data. With these corrections, scan position biases are reduced from as large as 8 K to less than 1 K for all scan positions and less than 0.4 K for all but the last few scan positions. Future ICWG investigations will focus on sources of and corrections for the remaining biases.

III. Conclusion

A method for end-to-end calibration of spaceborne radiometers using a combination of the vicarious cold and warm calibration techniques has been demonstrated using WindSat data. Using the method, brightness temperatures were corrected for attitude offsets as well as beam-spoiling due to interference from on-board sources near the radiometer edge-of-scan. The magnitude of the roll and pitch offset of the instrument as well as the beam fractions and effective radiating temperatures of the on-board obstructions were estimated.

References

[1] The GPM Intersatellite Calibration Working Group. [Online]. Available: http://www.gpm-x-cal.info/

[2] C. S. Ruf, "Detection of calibration drifts in spaceborne microwave radiometers using a vicarious cold reference," *IEEE Trans. Geosci. Remote Sens.*, vol. 38, no. 1, pp. 44–52, Jan. 2000.

[3] C. S. Ruf, Y. Hu, and S. T. Brown, "Calibration of windSat polarimetric channels with a vicarious cold reference," *IEEE Trans. Geosci. Remote Sens.*, vol. 44, no. 3, pp. 470–475, Mar. 2006.

[4] S. Brown and C. Ruf, "Determination of a hot blackbody reference target over the Amazon rainforest for the on-orbit calibration of microwave radiometers," *J. Atmos. Ocean. Technol.*, vol. 22, no. 9, pp. 1340–1352, Sep. 2005.

[5] P. Gaiser, K. M. St. Germain, E. M. Twarog, G. A. Poe, W. Purdy, D. Richardson, W. Grossman, W. L. Jones, D. Spencer, G. Golba, J. Cleveland, L. Choy, R. M. Bevilacqua, and P. S. Chang, "The Windsat spaceborne polarimetric microwave radiometer: Sensor description and early orbit performance," *IEEE Trans. Geosci. Remote Sens.*, vol. 42, no. 11, pp. 2347–2361, Nov. 2004.

[6] W. L. Jones, J. D. Park, S. Soisuvarn, L. Hong, P. W. Gaiser, and K. M. St. Germain, "Deep-space calibration of the WindSat radiometer," *IEEE Trans. Geosci. Remote Sens.*, vol. 44, no. 3, pp. 476–495, Mar. 2006.

[7] G. S. Elsaesser and C. K. Kummerow, "Towards a fully parametric retrieval of the non-raining parameters over the global oceans," *J. Appl. Meteorol. Climatol.*, vol. 47, no. 6, pp. 1599–1618, Jun. 2008.

[8] I. Corbella, A. J. Gasiewski, M. Klein, and J. R. Piepmeier, "Compensation of elevation angle variations in polarimetric brightness temperature measurements from airborne microwave radiometers," *IEEE Trans. Geosci. Remote Sens.*, vol. 39, no. 1, pp. 193–195, Jan. 2001.

[9] W. E. Purdy, P. W. Gaiser, G. A. Poe, E. A. Uliana, T. Meissner, and F. J. Wentz, "Geolocation and pointing accuracy analysis for the WindSat sensor," *IEEE Trans. Geosci. Remote Sens.*, vol. 44, no. 3, pp. 496–505, Mar. 2006.

[10] T. Meissner and F. J. Wentz, "Polarization rotation and the third Stokes parameter: The effects of spacecraft attitude and Faraday rotation," *IEEE Trans. Geosci. Remote Sens.*, vol. 44, no. 3, pp. 506–515, Mar. 2006.

[11] T. H. Zapotocny, J. A. Jung, J. F. Le Marshall, and R. E. Treadon, "A two-season impact study of satellite and in situ data in the NCEP global data assimilation system," *Weather Forecast.*, vol. 22, no. 4, pp. 887–909, Aug. 2007.

[12] C. Prigent, E. Jaumouilee, F. Chevallier, and F. Aires, "A parameterization of the microwave land surface emissivity between 19 and 100 GHz, anchored to satellite-derived estimates," *IEEE Trans. Geosci. Remote Sens.*, vol. 46, no. 2, pp. 344–352, Feb. 2008.

[13] M. C. Colton and G. A. Poe, "TOPEX/Poseidon microwave radiometer (TMR). II. Antenna pattern correction and brightness temperature algorithm," *IEEE Trans. Geosci. Remote Sens.*, vol. 33, no. 1, pp. 138–146, Jan. 1995.

[14] M. C. Colton and G. A. Poe, "Intersensor calibration of DMSP SSM/I's: F-8 to F-14, 1987-1997," *IEEE Trans. Geosci. Remote Sens.*, vol. 37, no. 1, pp. 418–439, Jan. 1999.

Darren S. McKague (M'08) received the Ph.D. degree in astrophysical, planetary, and atmospheric sciences from the University of Colorado, Boulder, in 2001.

He is an Assistant Research Scientist in the Department of Atmospheric, Oceanic & Space Sciences at the University of Michigan, Ann Arbor. Prior to working for Michigan, he worked as a Systems Engineer for Ball Aerospace and for Raytheon and as a Research Scientist at Colorado State University. His work has focused on remote sensing with emphases on the development of spaceborne microwave remote sensing hardware, passive microwave calibration techniques, and on mathematical inversion techniques for geophysical retrievals. His experience with remote sensing hardware includes systems engineering for several advanced passive and active instrument concepts and the design of the calibration subsystem on the Global Precipitation Mission (GPM) Microwave Imager (GMI) and the development of calibration techniques for the GPM constellation while at the University of Michigan. His algorithm experience includes the development of a near-real time algorithm for the joint retrieval of water vapor profiles, temperature profiles, cloud liquid water path, and surface emissivity for the Advanced Microwave Sounding Unit (AMSU) at Colorado State University, and the development of the precipitation rate, precipitation type, sea ice, and sea surface wind direction algorithms for the risk reduction phase of the Conical scanning Microwave Imager/Sounder (CMIS).

Christopher S. Ruf (S'85–M'87–SM'92–F'01) received the B.A. degree in physics from Reed College, Portland, OR and the Ph.D. degree in electrical and computer engineering from the University of Massachusetts, Amherst.

He is currently a Professor of atmospheric, oceanic, and space sciences; a Professor of electrical engineering and computer science; and Director of the Space Physics Research Laboratory, University of Michigan, Ann Arbor. He has worked previously at Intel Corporation, Hughes Space and Communication, the NASA Jet Propulsion Laboratory, Pasadena, CA and Penn State University, University Park. In 2000, he was a Guest Professor with the Technical University of Denmark, Lyngby, Denmark. He has published in the areas of microwave radiometer satellite calibration, sensor and technology development, and atmospheric, oceanic, land surface and cryosphere geophysical retrieval algorithms.

Dr. Ruf is a member of the American Geophysical Union (AGU), the American Meteorological Society (AMS) and Commission F of the Union Radio Scientifique Internationale, and a Fellow of the IEEE. He has served on the editorial boards of the AGU Radio Science, the IEEE Transactions on Geoscience and Remote Sensing (TGRS), and the AMS Journal of Atmospheric and Oceanic Technology. He is currently the Editor-in-Chief of TGRS. He has been the recipient of three NASA Certificates of Recognition and four NASA Group Achievement Awards, as well as the 1997 TGRS Prize Paper Award, the 1999 IEEE Resnik Technical Field Award, and the 2006 International Geoscience and Remote Sensing Symposium Prize Paper Award.

John J. Puckett (S'08) received the M.S. degree in electrical engineering and the M.S. degree in atmospheric and space science from the University of Michigan, Ann Arbor, in 2010. In 2007, he received his B.S. degree in physics from Northern Michigan University, Marquette.

He is currently a Concept Design Engineer at JST Corporation in Farmington Hills, Michigan. Prior to working at JST, he was employed as an engineer for the remote sensing group at the University of Michigan. As a student and employee at Michigan, John focused on airborne, ground based & spaceborne passive microwave remote sensing hardware applications as well as geophysical retrieval and data analysis. His major projects include Global Precipitation Measurement (GPM), Radio Frequency Survey of Earth (RISE) and the JUNO Microwave Calibration System (JUNO-MCS).